




Original Paper

Acoustic Emission and Energy Dissipation Characteristics of Gas-Bearing Coal Samples Under Different Cyclic Loading Paths

Qingmiao Li ¹, Yunpei Liang,^{2,3} Quanle Zou,² and Quangui Li^{2,3}

Received 9 January 2019; accepted 18 June 2019
Published online: 10 July 2019

Cyclic loading widely exists in coal mining activities, and it can significantly change the mechanical and seepage characteristics of coal. In this study, raw gas-bearing coal with different coal rank was mechanically tested under three stress paths: cyclic loading with stepwise increased peak stress (path 1), with step-by-step increased peak stress (path 2) and with crossed peak stress (path 3) using a tri-axial seepage testing machine. The acoustic emission (AE) signals under different loading and unloading paths indicate different mechanical properties of the coal sample. The Kaiser point is not a good indicator of the stress history of coal. The ratios of the quiet effect of the three coal samples under the three stress paths show that loading path 1 can increase defects such as micro-cracks in the coal samples (the AE quiet period decreases), while the other two paths decrease the number of defects (the AE quiet period increases). The cumulative dissipated energy of the coal shows an exponential growth with axial effective stress. The damping coefficient of coal first decreases then increases under cyclic loading. The damage variables can be used to predict the failure of coal samples, regardless of the stress path. Our results provide theoretical support and insight into the permeability increase mechanism and strengthened permeability increase mechanism of coal seams based on cyclic-loading-induced fracturing (repetitive hydraulic fracturing) under multiple protections and gas drainage engineering.

KEY WORDS: Cyclic loading, Acoustic emission, Felicity ratio, Energy dissipation, Damage.

INTRODUCTION

During coal mining activities, coal and rock mass are generally subjected to cyclic loads (Wang et al. 2018a, b). For example, in multiple protection projects where groups of coal seams are mined, coal in a protected seam is subjected to cyclic loading

(Fig. 1). This significantly changes the mechanical and seepage characteristics of the coal (Zou et al. 2015; Chang and Tian 2018; Li et al. 2018; Zou and Lin 2018; Wu et al. 2018; Peng et al. 2019) and has a strong influence on the instability and failure as well as damage characteristics of gas-bearing coal under complex stresses. Therefore, it is necessary to study the mechanical and energy dissipation characteristics of gas-bearing coal under different loading and unloading paths (Feng et al. 2018; Wang et al. 2018a, b).

Many researchers have conducted highly effective studies on the mechanical and permeability properties of coal under cyclic loading using various

¹State Key Laboratory of Geohazard Prevention and Geo-environment Protection, Chengdu University of Technology, Chengdu 610059, China.

²State Key Laboratory of Coal Mine Disaster Dynamics and Control, Chongqing University, Chongqing 400044, China.

³To whom correspondence should be addressed; e-mail: liangyunpei@126.com, liq@cqu.edu.cn

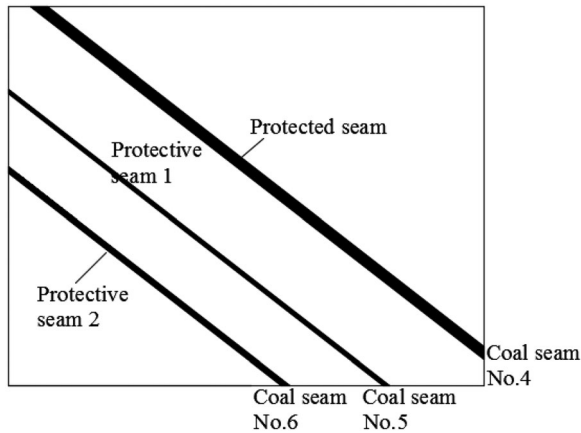


Fig. 1. Schematic diagram of multiple protection projects.

methods of analysis such as acoustic emission (AE), ultrasonic waves (Jia et al. 2019) and computed tomography (CT) (Cai et al. 2014). Additionally, energy dissipation theory (Liu et al. 2016) was applied to construct a constitutive model describing the damage in coal subjected to cyclic loading. AE is generated when materials or structures release strain energy rapidly in the form of transient elastic waves when they are deformed and damaged due to external or internal forces. Gas-bearing coal can produce multiple signals during the deformation and failure process. The signal produced during an AE event is most closely related to the mechanisms of micro-fracturing activities and is the most important physical method of determining a precursor of coal failure. Therefore, in this study, we investigated the AE characteristics of coal under cyclic loading. AE events in coal under cyclic loading can reflect the memory characteristics of the loading. When AE events are generated when the stress rises to a level previously exerted on the material, the phenomenon is known as the Kaiser effect, and the stress where the AE events are generated is the Kaiser point. When AE events appear when the loading stress is lower than the highest stress applied previously, it is known as the Felicity effect. AE can effectively record energy changes during micro-crack propagation in coal samples under cyclic loading. Yang et al. (2019) divided the processes of AE activity and energy dissipation in uniaxial cyclic loading of coal samples into three stages, but only the AE counts were analyzed. For processing of AE data, Zhang et al. (2018c) analyzed AE information of coal samples under cyclic loading by using the single-link clustering method and derived the relationship be-

tween coal loading and the resulting degradation. Shkuratnik et al. (2006) performed uniaxial cyclic loading tests on coal samples and analyzed the relationship between the AE data and stress memory, but they only studied the characteristics of a loop, the results of multiple loops are missing. Liang et al. (2017) monitored post-peak crack propagation and mechanical characteristics of rocks under cyclic loading using AE data. Furthermore, Yang et al. (2018a, b) measured AE data of coal samples under different stresses in real time and classified the data according to the failure types of coal. They showed that external stress influences the transition effects on the energy distribution of AE events and AE activity patterns. The theory of energy dissipation can well explain the failure process of coal under cyclic loading. AE information can reflect the type of coal rock damage, Zhang et al. (2018a, b, c) divided, according to the AE energy curve by using energy evolution in the failure of coal as an index, brittleness of coal into three types, i.e., fast fracturing, stable fracturing and plastic fracturing. Xue et al. (2018) studied the mechanical properties, AE characteristics and energy evolution characteristics of coal samples under mining stress. Ning et al. (2018) identified crack initiation and propagation thresholds in cyclic loading tests of coal by using a new energy dissipation method. Yin et al. (2015) obtained concentration coefficients of abutment stress in a working face at which a coupling experiment on mining-induced mechanical behavior and permeability evolution of coal was conducted in a complete deformation process. This research provides good reference for the analysis of coal and rock damage by AE, but the lack of analysis of AE Felicity effect under cyclic loading requires further research.

The occurrence of raw coal mass is usually associated with gas that affects its mechanical and permeability properties. Xie et al. (2017) conducted a uniaxial compression test on coal samples under different gas pressures and pointed out that coal strength decreases with increasing gas pressure, causing more severe crack damage. Yang et al. (2018a, b) studied the anisotropy of coal sample permeability through cyclic loading tests under different hydrostatic pressures. The results show that cyclic loading causes irreversible weakening of permeability. Zhang et al. (2018a) carried out cyclic loading tests on coal samples with a single crack and investigated the relationship between stress and permeability. The results showed that crushing,

redistribution and compressive deformation of fracture surfaces in the coal mass resulted in a dramatic decrease in permeability. Zhang and Zhang (2018) conducted different cyclic loading tests on gas-bearing coal samples with different combinations of coal particle sizes and studied the sensitivity of permeability to stress. Zou et al. (2016) investigated the influences of the effective stress on anisotropic permeability of coal under cyclic loads. The above studies on gas-bearing coal were conducted under a single cyclic path (Zhang and Zou 2018); however, the stress on coal in mining activities is very complex, especially in protected seams under multiple protections. Therefore, it is necessary to study the mechanical and energy dissipation properties of different gas-bearing coal samples under different cyclic loading paths.

In this study, we analyzed stress on coal in protected coal seams under multiple protections. We applied three simplified cyclic stress loading paths to gas-bearing coal collected from three sites, and tri-axial tests were conducted on the test samples. Based on the AE characteristics, we analyzed the fracturing characteristics of micro-cracks in the coal and then obtained and analyzed the energy dissipation characteristics of the coal samples under cyclic loads. Based on this, we derived a model for calculating coal degradation. The results provide theoretical support for modeling of the permeability increase mechanism and the strengthened permeability increase mechanism of coal seams based on cyclic-loading-induced fracturing (repetitive hydraulic fracturing) under multiple protections.

CYCLIC LOADING TEST

Test Equipment

The test was conducted by using a self-developed tri-axial seepage testing device that measures the thermo-hydro-mechanical coupling of gas-bearing coal. The device can be used for gas seepage testing of coal under different in situ stress fields (confining and axial pressures), gas pressures and temperature fields (Fig. 2).

Coal Samples

Three coal samples were taken from each of three sites: the Yuanzhuang coal mine in Anhui

province; the Gaohe coal mine in Shanxi province; the No. 10 coal mine of the Pingdingshan Coal Industry Group in Henan province, China. All samples were taken from the same piece of raw coal and were drilled in the same direction. The coal blocks drilled from the coal mines were cut and grinded into standard cylindrical coal samples with diameter of 50 mm and length of 100 mm. The properties of the three coal samples are listed in Table 1.

The heterogeneity of properties is mainly from defects in the coal. In order to reduce its impact on the test results, we tested the wave speed of every specimen by ultrasonic tester before the experiment. According to the wave speed test result (Fig. 3), three specimens with similar wave speed from the same piece of coal sample for every kind of coal were selected. Because wave velocity can well reflect the development of defects in coal and rock samples, similar wave speeds indicate that fracture development in samples is basically the same. Thus, the specimens selected for the study have similar mechanical and permeability properties in the initial state. These impart universal applicability of the study results (Shkuratnik et al. 2006; Peng et al. 2014a, b; Yin et al. 2015; Jiang et al. 2017; Khandelwal and Ranjith 2017; Xue et al. 2017; Zhang et al. 2018b, c; Yang et al. 2019).

Test Scheme

In order to get a reasonable load and unload path, we carried out a similarity simulation experiment on real-time monitoring of stress state of a protected seam on the mining conditions of a coal seam group. The simulation experiment model is shown in Figure 4. During the experiment, on the conditions when successively mining 5# and 6# coal seams, the stress state of the 4# coal seam was monitored in real time (Fig. 5). Before the 5# coal seam was mined for 80 m, the coal masses at the monitored point of the 4# coal seam were subjected to significant stress concentration. Furthermore, during the mining of the 6# coal seam, the coal masses at the monitored point of the 4# coal seam underwent multiple stress concentration and stress relief.

To study the damage and energy dissipation laws of gas-bearing coal under complex stresses, we designed three simplified stress paths (Li et al. 2018). The specific loading process was displayed as fol-

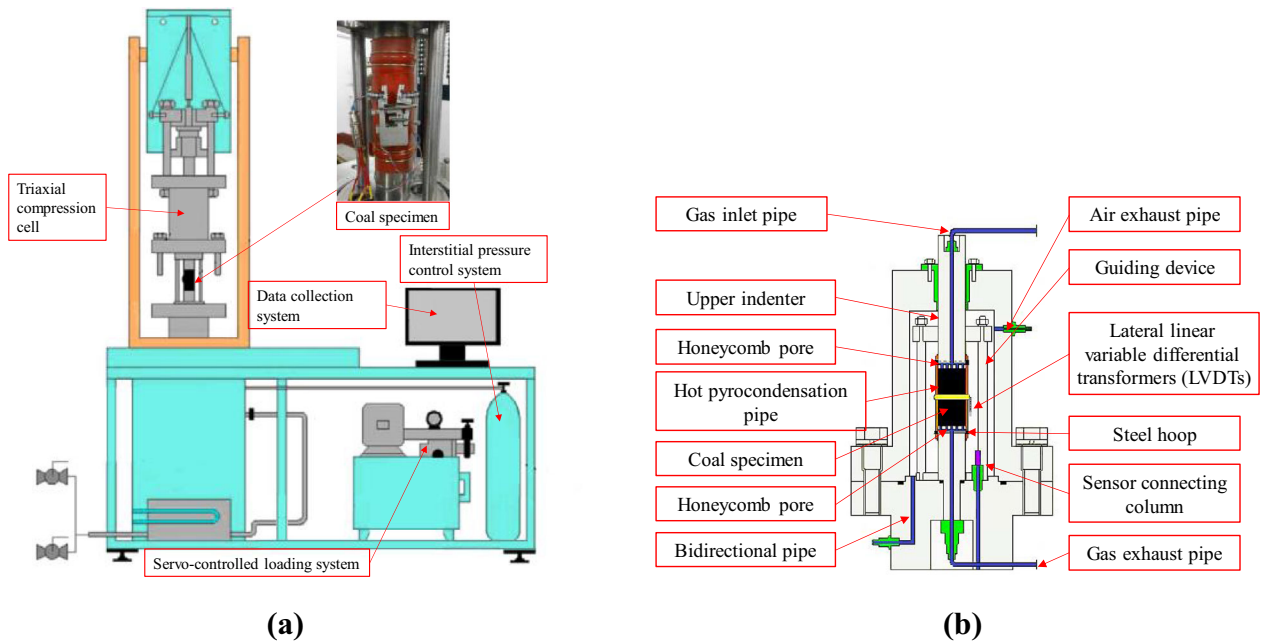


Fig. 2. Tri-axial seepage experimental device for the measurement of the heat–fluid–solid coupling property of gas-containing coal: (a) the whole experimental device; (b) the experimental chamber.

Table 1. Properties of coal samples

Sample	Water content (%)	Volatiles (%)	Ash content (%)	Fixed carbon (%)	Coal rank	Consistent coefficient	Initial permeability (mD)
Gaohe coal mine	1.11	27.71	5.32	65.9	Medium bituminous	0.65	3.5
No. 10 coal mine in Pingdingshan Coal Industry Group	1.30	29.55	10.88	56.61	Low-rank bituminous	0.49	5.5
Yuanzhuang coal mine	1.88	32.21	6.11	59.8	High bituminous	0.61	4

lows. The axial stress and confining pressure were increased to 2 MPa at a rate of 0.05 MPa/s under hydrostatic pressures, and then the testing chamber was filled with gas at a pressure of 1 MPa. The concentration of methane was 99.99%. The coal samples were kept for 24 h in this state to reach adsorption saturation. While the confining pressure remained unchanged, axial stress was applied or eased according to the loading pattern at a constant rate of 0.05 MPa/s until the coal samples failed. The three loading paths used in the test are shown in Figure 6. The effects of repeated loading and unloading paths on the raw coal samples were studied by analyzing the samples' permeability, energy dissipation and AE characteristics. The AE

count and AE energy parameters were studied in detail. The AE count refers to the number of pulses exceeding a set threshold and reflects the frequency of the AE events. The AE energy indicates the energy released during the AE event and shows the intensity of the event.

TEST RESULTS

Nine specimens were used for the tests; the coal samples from each of the three sites were tested under the three cyclic loading paths. The coal samples taken from the same coal block were assumed to have similar density, wave velocity and strength.

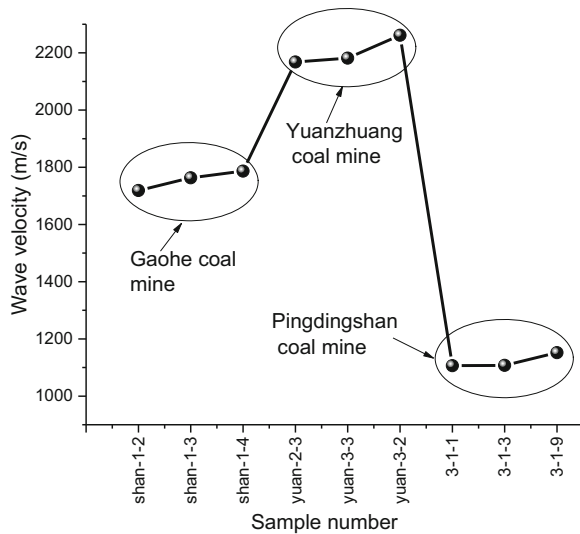


Fig. 3. Wave speeds of the chosen specimens.

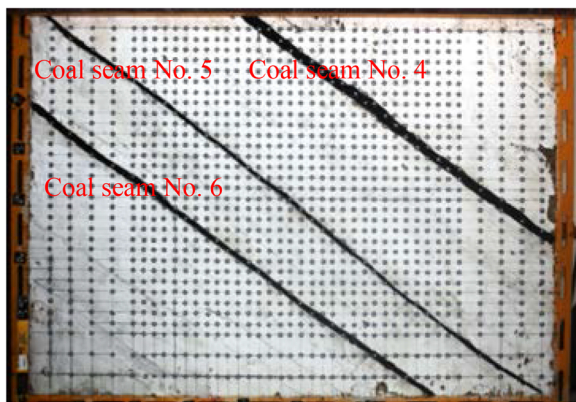


Fig. 4. Similarity model for real-time monitoring of stress state of protected seam under mining of multiple protective seams.

In the test on the Yuanzhuang coal samples under path 3, heat-shrinking tubes were pierced by the coal blocks, causing hydraulic oil to seep into the coal samples and damaging the sample. Therefore, only eight specimens were used for the analysis in this study.

As demonstrated in Figures 7, 8 and 9, as the number of cycles increased, the AE energy and AE count of the three types of coal samples under the three paths showed periodic growth. In addition, in the first cyclic loading stage of each sample, the defects, such as cracks and pores in the coal samples, are compacted and closed, generating AE signals. These signals disappear in the unloading stage. This phenomenon appears most clearly in the Gaohe coal

samples but does not appear in the Pingdingshan coal samples, indicating fewer initial defects and cracks in the latter samples. The AE signals in subsequent cycles appear mainly when the current stress exceeds the previous loading stress. There is a period with no AE activity before the failure of the coal. During the fracturing period of the coal, a sudden increase in the AE signals can be seen. Analysis of the AE data of per coal sample under cyclic loading is presented below.

Under stress path 1 (Fig. 6a), the axial stress shows a general stepwise increase during the cyclic loading test (Fig. 7). It increases in the loading and decreases to the peak of the previous cycle during the unloading; thus, some of the stress is retained after the loading and unloading, with the peak stress increasing stepwise. As shown in Figure 7, AE signals are still found in the stress-retaining sections of the Gaohe and Yuanzhuang coal samples. The slopes of the curves of the AE cumulative ring-down count and AE cumulative energy are larger than 0; however, the curve of the stress-retaining section of the Pingdingshan coal samples is almost horizontal. The AE count and AE energy of the three types of coal samples gradually rise as the stress levels increase and are the highest in the fracturing stage. The AE count and AE energy under path 1 reflect the gradually cumulative process of coal damage. The stress unloading restores some of the micro-crack deformation in the samples, while stress loading is still the main factor of crack propagation.

Under stress path 2 (Fig. 6b), the peak stresses in each cycle increase step-by-step and decrease to a hydrostatic pressure of 2 MPa between the peaks (Fig. 8). AE signals are produced in each loading and unloading cycle, and the AE count and energy gradually rise with the increased peak stress. The slopes of the curves of the accumulative AE count and cumulative AE energy increase suddenly before the final peak of each cycle. Similar to path 1, the AE activity of the Pingdingshan coal samples occurs during the unloading stage and the subsequent stress-retaining stage, while the other two types of coal samples still show AE clusters at this stage. This indicates that the mechanical properties of the Pingdingshan coal samples are different from those of the other samples; the micro-cracks in the Pingdingshan samples demonstrate stronger plastic characteristics. The test results of stress path 2 indicate that the unloading process is accompanied by deformation of the material defects such as micro-cracks, thus adding to the material degradation.

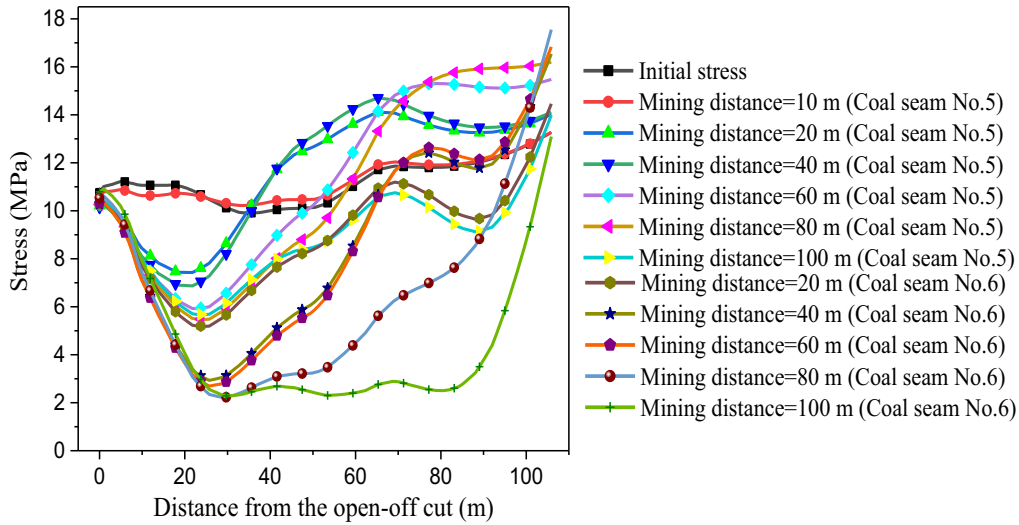


Fig. 5. Stress state in protected seam after mining of protective seams.

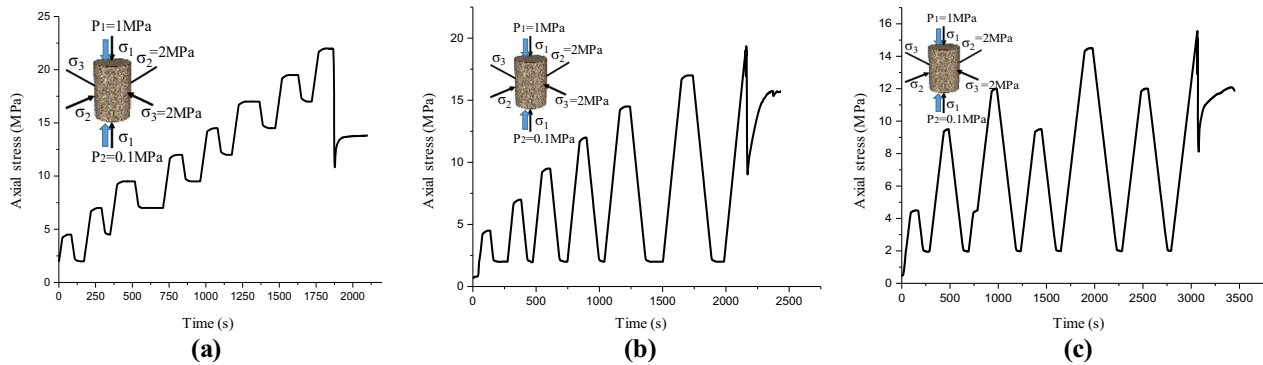


Fig. 6. Cyclic loading–unloading stress paths used for studying damage and energy dissipation laws of gas-bearing coal under complex stresses.

Based on stress path 2 (Fig. 6b), the peak stresses in each cycle were crossed under path 3 (Fig. 6c) in order to investigate the AE characteristics of coal under different degrees of loading and unloading (Fig. 9). The Pingdingshan coal samples show almost no AE events throughout the loading and unloading process when the peak stress of the cycle is equal to the previous peaks, and the curves of the cumulative AE count and cumulative AE energy are almost horizontal. This indicates that the deformation of the micro-cracks in the Pingdingshan coal samples has very strong plasticity characteristics and rarely recovers under unloading. Moreover, apart from during the highest stress peak, the cracks do not propagate even under loading; therefore, no AE is generated. For the Gaohe coal samples, AE events appear during loading and unloading, indi-

cating that the micro-cracks in the coal samples have stronger randomness and recover from the elastic deformation during the unloading process. The results under path 3 demonstrate that the coal samples from the different sites have different Kaiser effects.

DISCUSSION

Characteristics of Felicity Effects of AE Events for Different Gas-Bearing Coal Samples Under Cyclic Loading

The Felicity ratio F_R can be used to determine whether these two effects are significant or not. F_R can be expressed as follows:

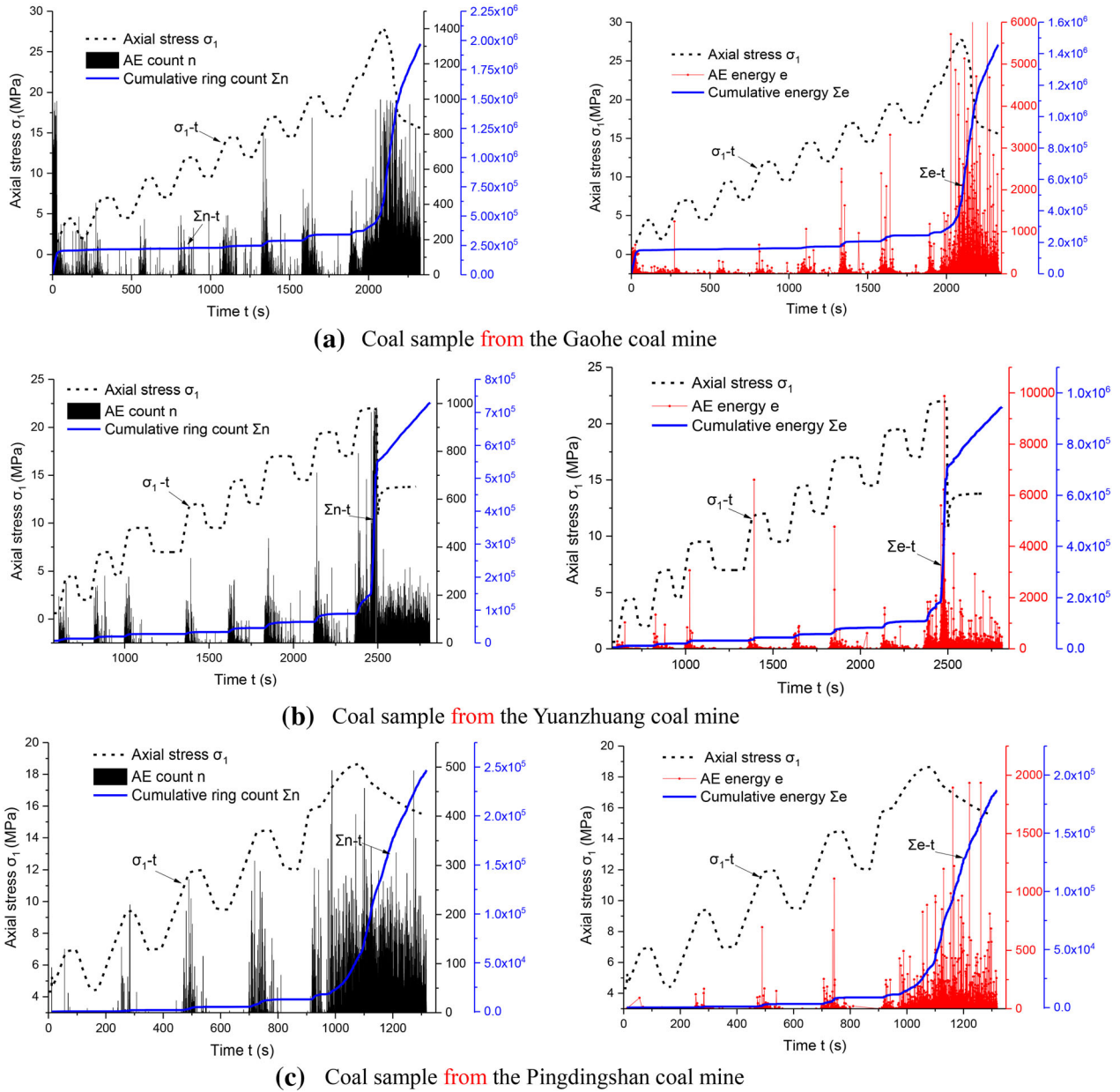


Fig. 7. AE count (black line) and AE energy (red line) for the three types of coal samples with stress (dashed line) under path 1 (Fig. 6a).

$$F_R = \frac{\sigma_k}{\sigma_p} \quad (1)$$

where σ_p and σ_k represent the maximum stress (in MPa) applied previously and the subsequent stress corresponding to the appearance of the AE event, respectively. The closer F_R is to 1, the more accurate is the memory of the material. When $F_R=1$, the coal stress memory lags behind; otherwise, the stress

memory is advanced. As shown in Figure 10, the F_R curves of the three types of coal samples under different loading and unloading paths show different trends, with the curves for path 1 being significantly different from those under loading paths 2 and 3.

Under stress path 1 (Fig. 6a), the F_R of the Gaohe coal samples under cyclic loading first increases and then stabilizes at $F_R \approx 1$. This indicates that defects such as pores, cracks and joints in the

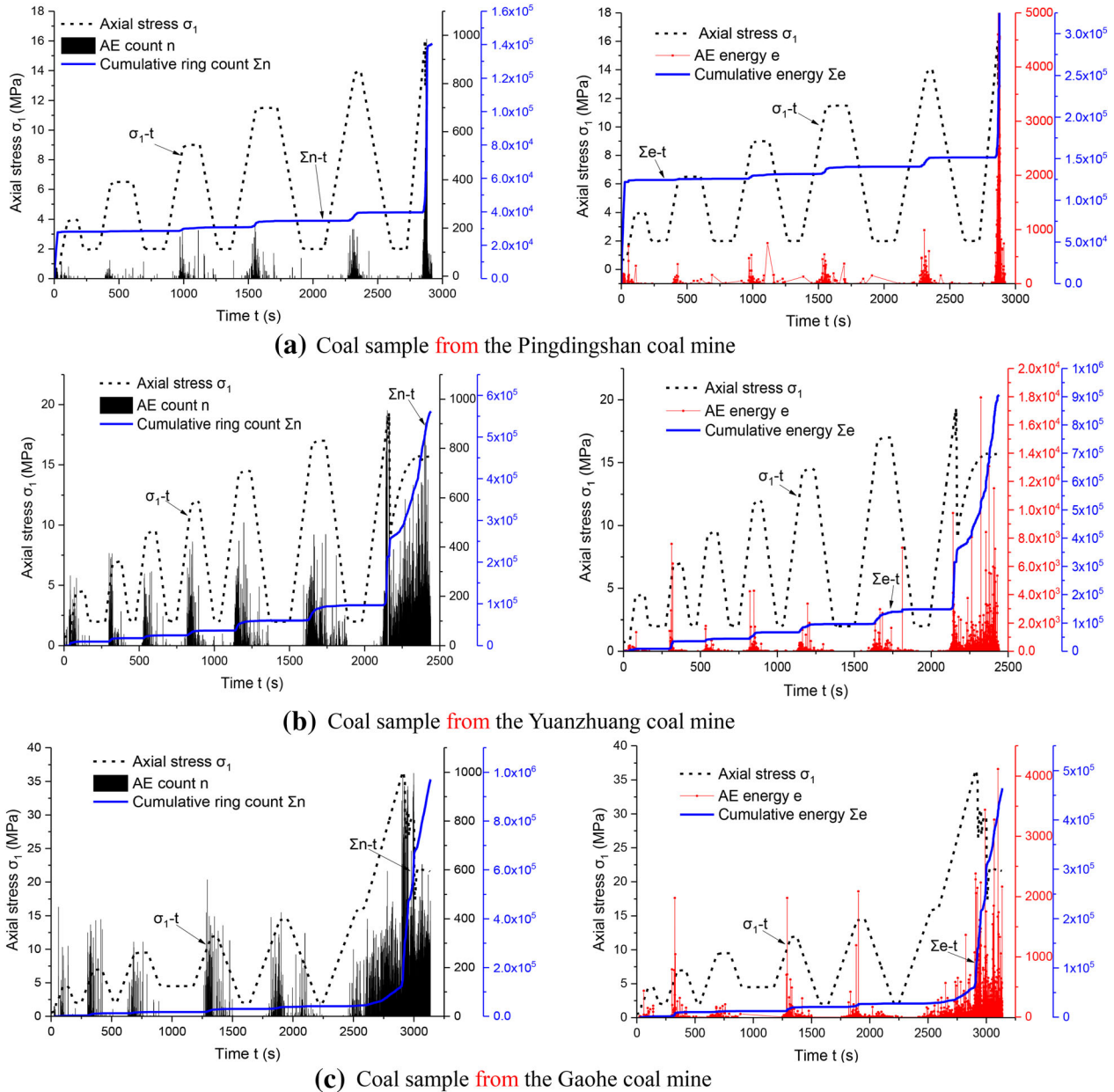


Fig. 8. AE count (black line) and AE energy (red line) of different coal samples with stress (dashed line) under stress path 2 (Fig. 6b).

coal samples are compacted and closed in the second and third cycles before reaching the stress applied in the previous cycle, thus generating irreversible deformation and releasing AE signals. In subsequent cyclic loading, the coal shows good stress memory characteristics. In the Yuanzhuang coal samples, F_R is always around 1, implying that the coal suffers less damage, develops fewer defects and has good stress memory characteristics. For the Pingdingshan coal

samples, $F_R > 1$, indicating that the coal demonstrates lagged stress memory and more obvious plasticity and heterogeneity.

Under stress path 2 (Fig. 6b), the F_R of the Gaohe coal sample first rises to around 1 and then decreases to about 0.9 as the cyclic loads are applied. This demonstrates that the pores, cracks and joints in the coal samples are constantly compacted and closed in the second and third cycles, thus generating

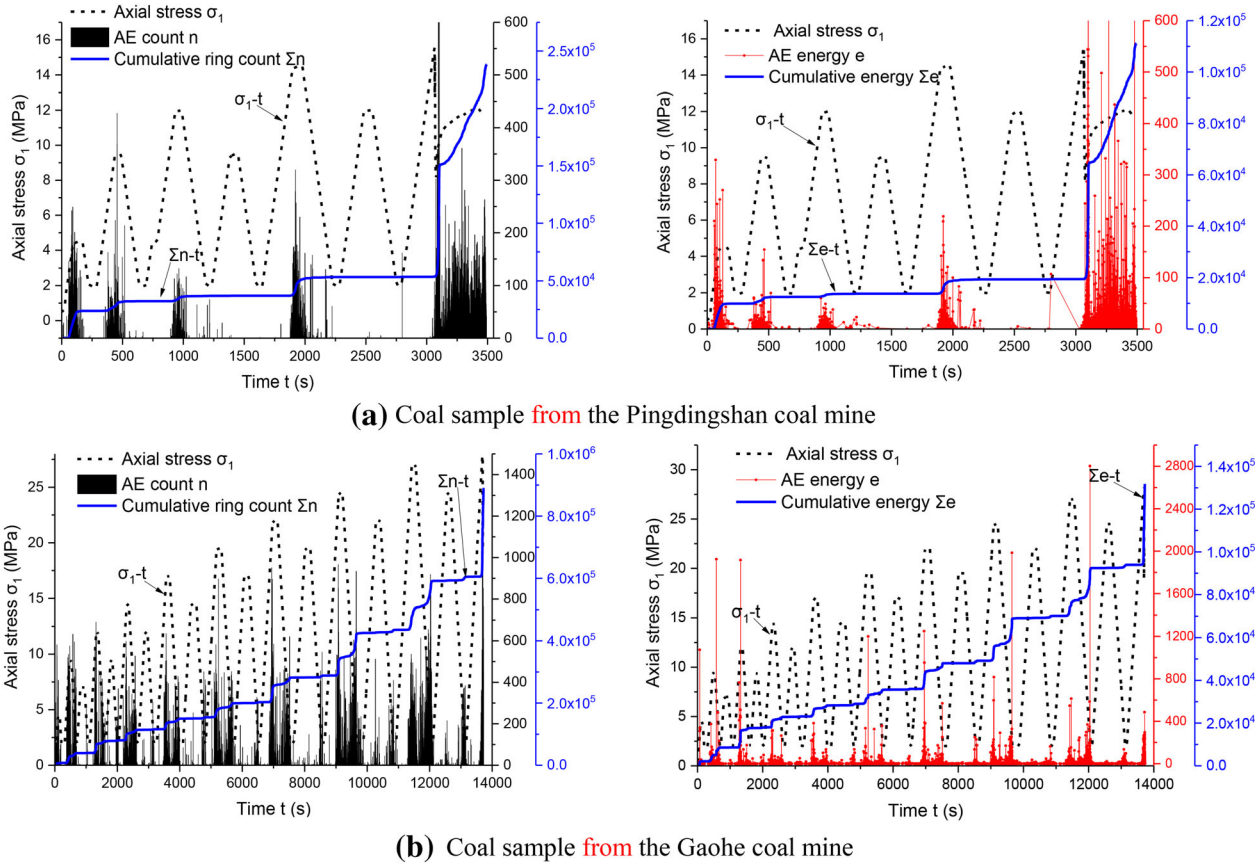


Fig. 9. AE count (black line) and AE energy (red line) for different coal samples with stress (dashed line) under stress path 3 (Fig. 6c).

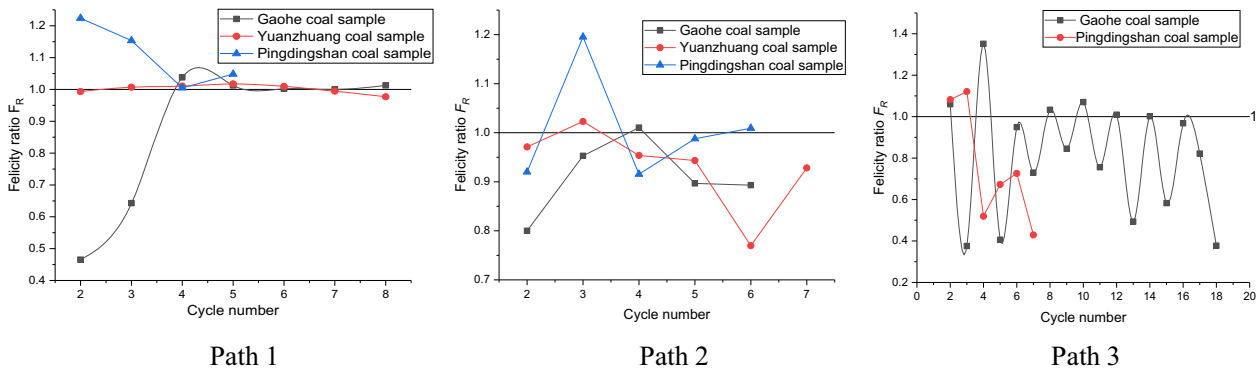


Fig. 10. Felicity ratios of the three types of coal samples under different loading and unloading paths.

irreversible deformation and releasing AE signals. Under subsequent cyclic loading, new cracks and defects are continuously created in the coal and excellent characteristics of stress memory are shown. The F_R curves of the Yuanzhuang and Gaohe coal

samples have similar trends and the F_R in the sixth cycle is 0.76, implying that the damage in the coal samples generated during the cyclic loading is constantly accumulated and the stress memory is continuously enhanced. The F_R of the Pingdingshan

coal samples has a trend similar to those of the samples from the other two sites, and the final ratio of the cycles is approximately 1, indicating that the cyclic loading has weakened the enhanced characteristics of the stress memory of the coal rocks.

Under stress path 3 (Fig. 6c), the F_R curve of the Gaohe coal samples fluctuates below 1 under cyclic loading. When the cycle stress peak is lower than in the previous cycle, the F_R in this cycle is smaller than that in the previous cycle. In the final damage stage under cyclic loading, F_R reaches its minimum. This demonstrates that the stress memory performance of the coal is affected by the loading and unloading history and that the stress history of the coal cannot be well determined through the Kaiser point. The Pingdingshan coal samples present F_R trends similar to those of the coal samples from the other two sites.

In summary, the stress paths influence the stress memory characteristics of coal and different types of coal samples under the same stress path show different stress memory characteristics. Therefore, one should be cautious when predicting the stability of coal mass based on the Kaiser effect.

The ratio of the subsequent stress when the AE signals appear in the loading stage to that when the AE signals disappear at the unloading stage (i.e.,) the 'quiet period effect' ratio, is

$$A_R = \frac{\sigma_k}{\sigma_n} \quad (2)$$

where σ_n indicates the stress when the AE signals disappear in the previous unloading. The basis for determining whether the AE signals disappear in the unloading and strengthen in the loading is the AE signal amplitude threshold of 60 dB (Zhang et al. 2006). $A_R < 1$ indicates that the coal material did not produce AE signals soon after unloading, but generated AE signals soon after reloading. This implies that the material has strong plasticity and the micro-cracks that opened due to the loading did not fully recover in the unloading process. These cracks constantly open and slip when subjected to small loads again, thus generating fracturing signals. $A_R \geq 1$ indicates that AE signals are still being generated in the coal during the unloading stage and continuing at a slower rate during reloading. This demonstrates that the materials are highly elastic and that micro-cracks opening during the loading quickly recover during unloading. Larger loads are then required during reloading to reopen the micro-

cracks. Thus, A_R reflects the loading-induced deformation and fracturing characteristics of the micro-cracks in the material to some extent.

A_R for the three types of coal samples under the three stress paths show a regular pattern (Fig. 11). Under cyclic loading path 1 (Fig. 6a), the A_R curve of the Gaohe coal samples first rises and then falls to around 1, demonstrating that the plasticity of the coal samples strengthens in the second and third cycles. When the cyclic load is applied, the elasticity of the materials gradually strengthens; thus, the cyclic loads first strengthen and then weaken the coal. The A_R values of the Yuanzhuang and Pingdingshan coal samples are always larger than 1 and gradually decrease with cyclic loading, indicating that the strengths of the two coal samples gradually decrease under cyclic loading.

Under stress path 2 (Fig. 6b), the A_R curves of the three types of coal samples increased with the number of cycles. This indicates that as the cyclic loads increased step-by-step they weakened the micro-crack propagation and deformation of the coal samples. Thus, the elasticity of the coal samples was enhanced and the quiet period of AE becomes gradually longer.

Under cyclic loading path 3 (Fig. 6c), the A_R curves of the two types of coal samples show an increasing trend with a few peaks and A_R is always greater than 1. This is because the cyclic loading with alternating peak stress changes the quiet period of the AE signals and enhances the elasticity of the coal samples.

The above results demonstrate that cyclic loading path 3 with stepwise increasing peak stress enhances defects, such as micro-cracks, in the coal samples (the quiet period of AE shortens), while the other two stress paths play a weakening role (the quiet period of AE becomes longer).

Energy Dissipation Characteristics of Coal Under Cyclic Loading

Because coal dissipates energy under cyclic loading, the damage process of coal can be analyzed by quantifying the energy dissipation (Peng et al. 2014a, b). During loading, energy accumulation and dissipation occur in the material, finally resulting in failure of the material. In the loading process, due to the influences of external forces, coal deformation occurs. The total work done by the external force on the coal samples is the total energy U , which is

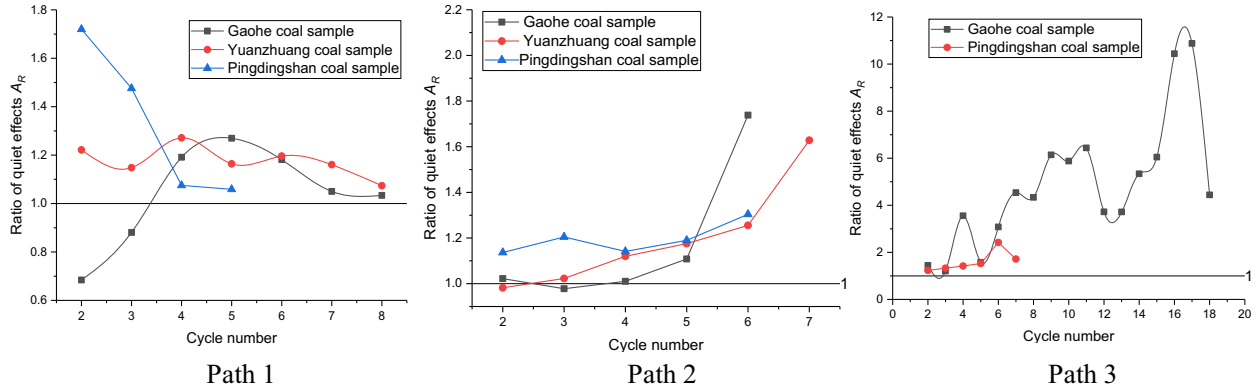


Fig. 11. The ‘quiet effect’ ratio of the three types of coal under different loading and unloading paths.

stored in the coal in the form of elastic potential energy E_e . Some of this energy, E_d , is lost through various forms of damage and dissipation. During unloading, elastic potential energy is released. This part of the energy is almost equal to the negative work E_r done by the external force during unloading. Thus:

$$U = E_e + E_d = E_r + E_d \quad (3)$$

In the loading and unloading test on gas-bearing coal mass, the influences of gas pressure on the axial stress and confining pressure should be considered when studying the energy of coal and rock mass. The forces that actually act on the coal mass are the axial effective stress and confining pressure. The axial effective stress (Terzaghi and Peck 1996) can be defined as

$$\sigma'_1 = \sigma_1 - \delta_{ij}p_1 \quad (4)$$

where σ'_1 , σ_1 , δ_{ij} and p_1 represent axial effective stress (in MPa), axial stress (in MPa), Kronecker delta and gas pressure (in MPa), respectively. In the loading and unloading test, the confining pressure is kept constant. During the loading and unloading process, the work done by the effective confining pressure on coal mass is far smaller than that of the axial effective stress. Therefore, we can ignore the work of the effective confining stress and analyze only the work done by the axial effective stress on the coal mass.

Taking the second loading and unloading cycle of the Pingdingshan coal samples under stress path 2 as an example, the dissipated energy was calculated (Fig. 12). The area under the curve $A'ABB'$ repre-

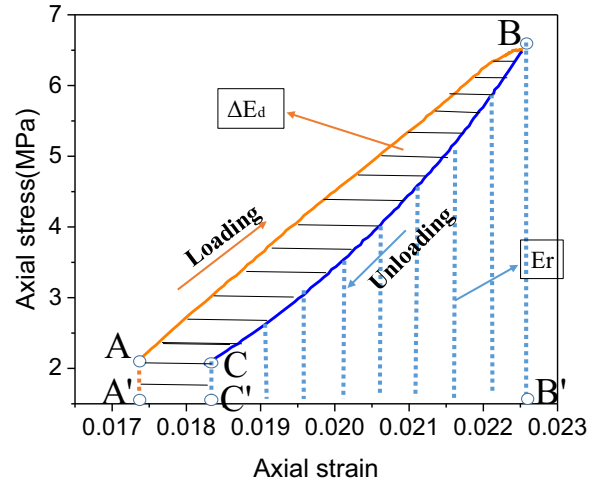


Fig. 12. Energy calculation for coal under cyclic loading and unloading conditions.

sents the total work U done by the axial effective stress in the loading process, while the area under the curve $C'CB B'$ indicates the elastic potential energy E_e that can be released in the unloading process of the axial effective stress. In the energy dissipation process, the area bound by the hysteresis is a loop. The area enclosed by the axial effective stress–strain curve can be calculated by integrating the stresses inside the area. Therefore, the total energy in the loading process can be calculated based on Eq. (5) (Jiang et al. 2017):

$$U = \int \sigma'_1 d\varepsilon_1 = \sum_{i=1}^n \frac{1}{2}(\sigma_{1i}^+ + \sigma_{1i-1}^+ - 2\delta_{ij}p_1)(\varepsilon_{1i}^+ - \varepsilon_{1i-1}^+) \quad (5)$$

Similarly, the elastic energy E_e released in the unloading process can be calculated as

$$E_e = \sum_{i=1}^n \frac{1}{2} (\sigma_{1i}^- + \sigma_{1i-1}^- - 2\delta_{ij}p_1) (\varepsilon_{1i}^- - \varepsilon_{1i-1}^-) \quad (6)$$

where, σ_{1i}^+ and ε_{1i}^+ represent the stress and strain at each point on the stress–strain curve in the loading stage, respectively, while σ_{1i}^- and ε_{1i}^- indicate the stress and strain at each point on the stress–strain curve in the unloading stage. Moreover, p_1 denotes the inlet pressure (in MPa) applied on the coal samples, with $p_1 = 1$ MPa in this test.

The cumulative dissipated energy can be obtained by summing all the areas of the hysteresis loop in each period. Because the elastic energy is not released completely under stress path 1, the actual dissipated energy cannot be obtained according to the above calculation method. Therefore, in this work, we only studied the behavior of the dissipated energy of the three types of coal samples under stress paths 2 and 3. Figure 13 presents the cumulative dissipated energy curves of the three types of coal samples under stress path 2 with increasing effective stress. The cumulative dissipated energy of the coal samples shows an exponential growth with axial effective stress because the increase in axial stress accelerates the failure of the coal under cyclic loading. Friction, secondary crack propagation and plastic deformation of coal and rock mass can raise energy dissipation. As displayed in Figure 13, the cumulative dissipated energy under stress path 3 ri-

ses as the alternating peak cyclic load is applied. The dissipated energy under the same peak load in the second cycle is smaller than that in the first cycle. However, the overall trend of the cumulative dissipated energy with increasing effective stress is still an exponential curve and the three types of coal show similar behavior.

The best-fit curve that describes the relationship between the cumulative dissipated energy and axial effective stress (Figs. 13 and 14) is an exponential function (Eq. 7):

$$E_d = a \exp[b(\sigma_1 - \delta_{ij}p_1)] \quad (7)$$

where E_d represents the cumulative dissipated energy (in MPa) and a and b are the fitting parameters. The damping coefficient refers to the ratio of the dissipated energy to the maximum strain energy in a loading and unloading cycle (Jiang et al. 2017):

$$\lambda = \frac{\Delta E_d^i}{U_{\max}^i} \quad (8)$$

where λ , ΔE_d^i and U_{\max}^i represent the damping coefficient, the dissipated energy in the i th cycle and the maximum strain energy in the i th cycle, respectively. The damping coefficient λ can be used to characterize the inelastic response and dissipation of a coal sample. The larger the damping coefficient, the more obvious the inelastic deformation of the coal. For an ideal elastomer, $\lambda = 0$. Figures 15 and 16 demonstrate similar λ curves for the three coal types under two cyclic loading stress paths (paths 2

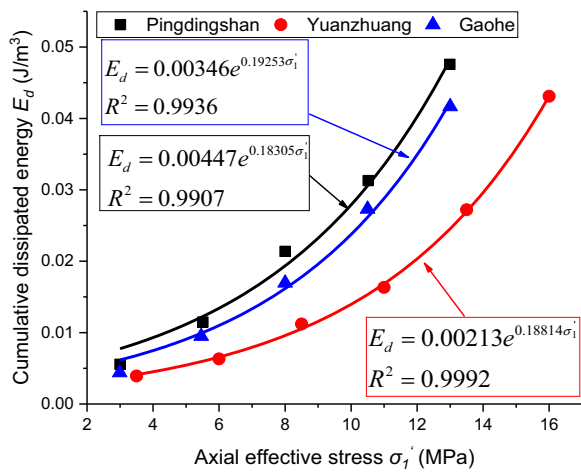


Fig. 13. Curves of dissipated energy of three coal types under stress path 2.

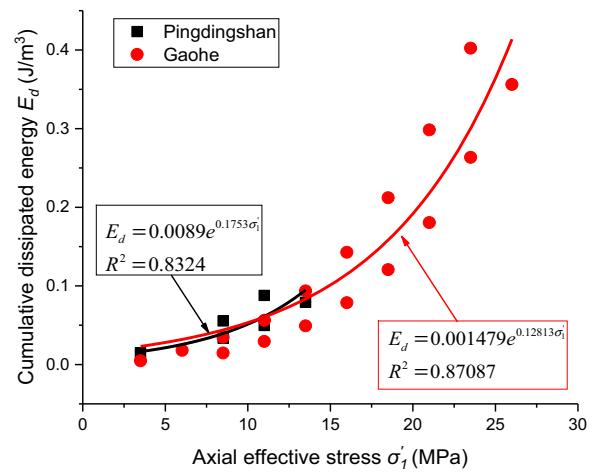


Fig. 14. Curves of dissipated energy of two types of coal samples under stress path 3.

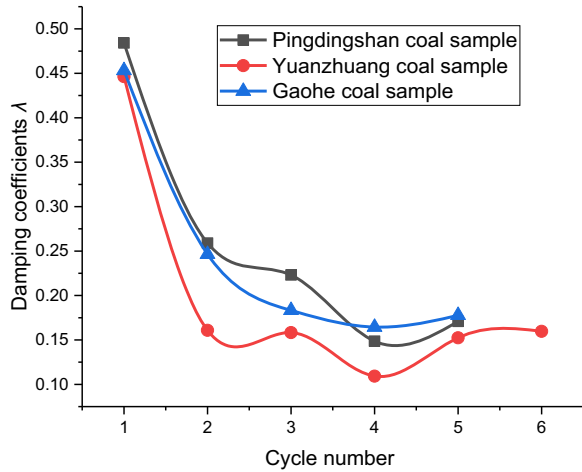


Fig. 15. Damping coefficients λ of the three types of coal samples under path 2.

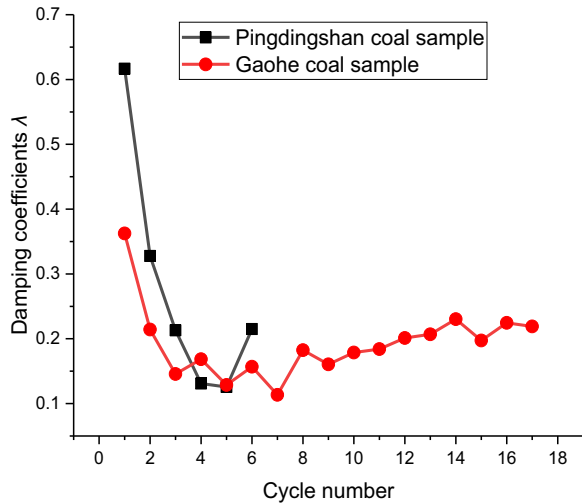


Fig. 16. Damping coefficients λ of two types of coal samples under path 3.

and 3). The λ of the coal samples first decreased and then increased slightly, indicating an initial weakening of the coal inelasticity followed by some strengthening. When λ reaches its minimum value, the inelasticity of the coal is most obvious. As the cyclic load continues, the degree of closure of pores and cracks in the coal samples, and the compaction and rigidity of the coal samples increase, while the area of the stress–strain hysteresis loop gradually decreases, that is, the energy consumed in a cycle decreases, thus reducing the damping ratio.

Damage Evolution Law

The AE characteristics and energy dissipation of gas-bearing coal under cyclic loading are the basic outcomes of the damage to coal, indicating coal degradation. To characterize the damage evolution in coal under cyclic loading, Peng et al. (2014a, b) proposed the variable D , which expresses the damage:

$$D = \frac{2}{\pi} \arctan \frac{\Delta E_d}{\Delta \sigma_1} \tag{9}$$

where ΔE_d and $\Delta \sigma_1$ represent the increments of dissipated energy and axial stress, respectively. When the dissipated energy is zero ($\Delta E_d = 0$), the coal samples are not damaged ($D = 0$). When the dissipated energy is infinite ($\Delta E_d \rightarrow \infty$), the coal samples have completely failed ($D = 1$), although in practice, the dissipated energy is not infinite. When the dissipated energy reaches a critical value, the coal samples are damaged; the damage variable under this condition is denoted D_c . When $D \geq D_c$, the coal samples are completely damaged. Generally, $D_c < 1$.

$$E_d = a \exp[b(\sigma_1 - \delta_{ij}p_1)] \tag{10}$$

By combining Eqs. 9 and 10, the damage variable can be expressed:

$$D = \frac{2}{\pi} \arctan\{ab \exp[b(\sigma_1 - p_1)]\} \tag{11}$$

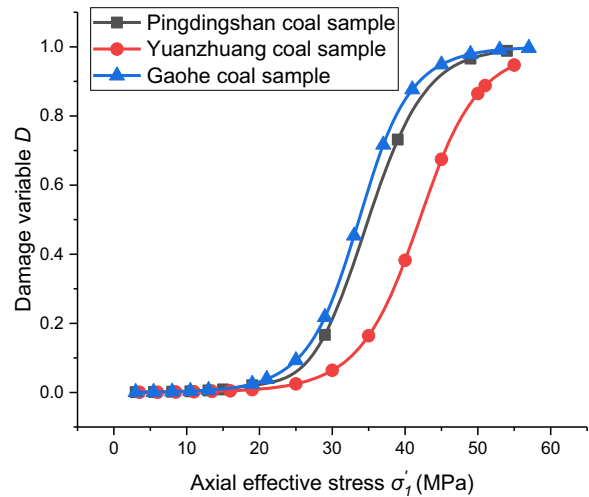


Fig. 17. Damage variable D of the three types of coal samples under stress path 2.

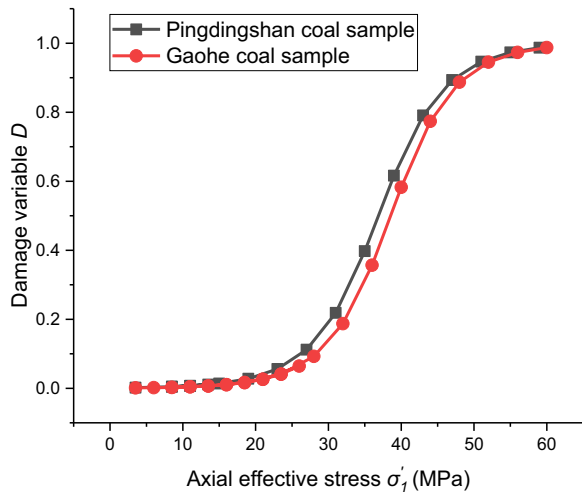


Fig. 18. Damage variable D of two types of coal samples under stress path 3.

Equation 11 presents the damage variable of coal samples under any axial effective stress, as demonstrated in Figures 17 and 18. Under cyclic loading, the peak axial effective stress increases and D of the coal samples rises. In addition, the coal samples are damaged more significantly. The three types of coal samples have different damage points (Fig. 17). The Yuanzhuang coal samples have higher strength than those of the other two coal samples, and the damage curves of the Pingdingshan and Gaohe coal samples are similar. Under path 3, the curves of the two coal types are similar, indicating that D can be used to predict the failure of the coal samples without being affected by the stress path.

CONCLUSIONS

To study the failure and energy evolution of different types of gas-bearing coal under complex stress conditions, we conducted cyclic loading tests on three types of gas-bearing coal samples under three different stress paths. By monitoring the failure process of the coal in real time through AE, this study analyzed the Felicity effects and energy dissipation laws and obtained the curve of the damage variable. The main conclusions are as follows.

1. As the number of loading cycles increased, the AE energy and count of the three types of coal samples with different coal rank all showed a periodic increase under the three

paths. The AE signals under different loading and unloading paths indicate different mechanical properties of the coal sample.

2. Under the three cyclic stress paths, the Felicity ratios of the different coal types had distinct trends with increased number of cycles. The Kaiser point is not a good indicator of the stress history of coal. The ratios of the quiet effects of the three coal samples under the three paths indicate that cyclic loading with stepwise increased peak stress can enhance defects such as micro-cracks in the coal samples (the AE quiet period decreases). Under the other two stress paths, the amount of defects such as micro-cracks decreases (the AE quiet period rises).
3. The cumulative dissipated energy curves of the three types of coal samples with effective stress under stress paths 2 and 3 show an exponential increase with axial effective stress. Under cyclic loading, the damping coefficient of the coal first decreases and then rises.
4. Coal degradation and failure under cyclic loading are expressed by the AE characteristics and energy dissipation of the gas-bearing coal. The critical damage points of the three coal samples are different. The damage variable can be used to predict the failure of the coal samples without being influenced by the stress path.

ACKNOWLEDGMENTS

This work is financially supported by the State Key Research Development Program of China (2017YFC0804206 and 2016YFC0801404), the National Natural Science Foundation of China (51674050 and 51704046), the National Science and Technology Major Project of China (2016ZX05043005), the Fundamental Research Funds for the Central Universities (2018CDQYZH0001 and 106112017CDJXY240001) and the Open Fund Research Project of State Key Laboratory Breeding Base for Mining Disaster Prevention and Control (MDPC201710). The authors thank the editor and anonymous reviewers very much for their valuable advices.

REFERENCES

- Cai, Y., Liu, D., Mathews, J. P., Pan, Z., Elsworth, D., Yao, Y., et al. (2014). Permeability evolution in fractured coal—Combining triaxial confinement with X-ray computed tomography, acoustic emission and ultrasonic techniques. *International Journal of Coal Geology*, *122*, 91–104. <https://doi.org/10.1016/j.coal.2013.12.012>.
- Chang, X., & Tian, H. (2018). Technical scheme and application of pressure-relief gas extraction in multi-coal seam mining region. *International Journal of Mining Science and Technology*, *28*(3), 483–489. <https://doi.org/10.1016/j.ijmst.2018.03.010>.
- Feng, J., Wang, E., Chen, X., & Ding, H. (2018). Energy dissipation rate: An indicator of coal deformation and failure under static and dynamic compressive loads. *International Journal of Mining Science and Technology*, *28*(3), 397–406. <https://doi.org/10.1016/j.ijmst.2017.11.006>.
- Jia, H., Wang, E., Song, D., Wang, X., & Ali, M. (2019). Precursory changes in wave velocity for coal and rock samples under cyclic loading. *Results in Physics*, *12*, 432–434. <https://doi.org/10.1016/j.rinp.2018.11.096>.
- Jiang, C., Duan, M., Yin, G., Wang, J. G., Lu, T., Xu, J., et al. (2017). Experimental study on seepage properties, AE characteristics and energy dissipation of coal under tiered cyclic loading. *Engineering Geology*, *221*, 114–123. <https://doi.org/10.1016/j.enggeo.2017.03.005>.
- Khandelwal, M., & Ranjith, P. G. (2017). Study of crack propagation in concrete under multiple loading rates by acoustic emission. *Geomechanics and Geophysics for Geo-Energy and Geo-Resources*, *3*(4), 393–404. <https://doi.org/10.1007/s40948-017-0067-1>.
- Li, Q., Liang, Y., & Zou, Q. (2018). Seepage and damage evolution characteristics of gas-bearing coal under different cyclic loading–unloading stress paths. *Processes*. <https://doi.org/10.3390/pr6100190>.
- Liang, Y., Li, Q., Gu, Y., & Zou, Q. (2017). Mechanical and acoustic emission characteristics of rock: Effect of loading and unloading confining pressure at the postpeak stage. *Journal of Natural Gas Science and Engineering*, *44*, 54–64. <https://doi.org/10.1016/j.jngse.2017.04.012>.
- Liu, X. S., Ning, J. G., Tan, Y. L., & Gu, Q. H. (2016). Damage constitutive model based on energy dissipation for intact rock subjected to cyclic loading. *International Journal of Rock Mechanics and Mining Sciences*, *85*, 27–32. <https://doi.org/10.1016/j.ijrmms.2016.03.003>.
- Ning, J., Wang, J., Jiang, J., Hu, S., Jiang, L., & Liu, X. (2018). Estimation of crack initiation and propagation thresholds of confined brittle coal specimens based on energy dissipation theory. *Rock Mechanics and Rock Engineering*, *51*(1), 119–134. <https://doi.org/10.1007/s00603-017-1317-9>.
- Peng, R. D., Ju, Y., Gao, F., Xie, H.-P., & Wang, P. (2014a). Energy analysis on damage of coal under cyclical triaxial loading and unloading conditions. *Meitan Xuebao/Journal of the China Coal Society*, *39*(2), 245–252. <https://doi.org/10.13225/j.cnki.jccs.2013.2010>.
- Peng, R., Ju, Y., Wang, J. G., Xie, H., Gao, F., & Mao, L. (2014b). Energy dissipation and release during coal failure under conventional triaxial compression. *Rock Mechanics and Rock Engineering*, *48*(2), 509–526. <https://doi.org/10.1007/s00603-014-0602-0>.
- Peng, K., Liu, Z., Zou, Q., Zhang, Z., & Zhou, J. (2019). Static and dynamic mechanical properties of granite from various burial depths. *Rock Mechanics and Rock Engineering*. <https://doi.org/10.1007/s00603-019-01810-y>.
- Shkuratnik, V. L., Filimonov, Y. L., & Kuchurin, S. V. (2006). Acoustic emission memory effect in coal samples under uniaxial cyclic loading. *Journal of Applied Mechanics and Technical Physics*, *47*(2), 236–240. <https://doi.org/10.1007/s10808-006-0048-6>.
- Terzaghi, K., & Peck, R. B. (1996). *Soil mechanics in engineering practice* (Vol. 142, pp. 149–150). Hoboken: Wiley.
- Wang, Y., Guo, P., Dai, F., Li, X., Zhao, Y., & Liu, Y. (2018a). Behavior and modeling of fiber-reinforced clay under triaxial compression by combining the superposition method with the energy-based homogenization technique. *International Journal of Geomechanics*. [https://doi.org/10.1061/\(asce\)gm.1943-5622.0001313](https://doi.org/10.1061/(asce)gm.1943-5622.0001313).
- Wang, J., Song, W., Cao, S., & Tan, Y. (2018b). Mechanical properties and failure modes of stratified backfill under triaxial cyclic loading and unloading. *International Journal of Mining Science and Technology*. <https://doi.org/10.1016/j.ijmst.2018.04.001>.
- Wu, F., Chen, J., & Zou, Q. (2018). A nonlinear creep damage model for salt rock. *International Journal of Damage Mechanics*. <https://doi.org/10.1177/1056789518792649>.
- Xie, G., Yin, Z., Wang, L., Hu, Z., & Zhu, C. (2017). Effects of gas pressure on the failure characteristics of coal. *Rock Mechanics and Rock Engineering*, *50*(7), 1711–1723. <https://doi.org/10.1007/s00603-017-1194-2>.
- Xue, Y., Dang, F., Cao, Z., Du, F., Ren, J., Chang, X., et al. (2018). Deformation, permeability and acoustic emission characteristics of coal masses under mining-induced stress paths. *Energies*, *11*(9), 2233.
- Xue, Y., Ranjith, P. G., Gao, F., Zhang, D., Cheng, H., Chong, Z., et al. (2017). Mechanical behaviour and permeability evolution of gas-containing coal from unloading confining pressure tests. *Journal of Natural Gas Science and Engineering*, *40*, 336–346. <https://doi.org/10.1016/j.jngse.2017.02.030>.
- Yang, Y. J., Duan, H. Q., Xing, L. Y., & Deng, L. (2019). Fatigue characteristics of coal specimens under cyclic uniaxial loading. *Geotechnical Testing Journal*. <https://doi.org/10.1520/gtj20170263>.
- Yang, D. S., Qi, X. Y., Chen, W. Z., Wang, S. G., & Yang, J. P. (2018a). Anisotropic permeability of coal subjected to cyclic loading and unloading. *International Journal of Geomechanics*, *18*(8), 8. [https://doi.org/10.1061/\(asce\)gm.1943-5622.0001229](https://doi.org/10.1061/(asce)gm.1943-5622.0001229).
- Yang, H., Wen, G., Hu, Q., Li, Y., & Dai, L. (2018b). Experimental investigation on influence factors of acoustic emission activity in coal failure process. *Energies*, *11*(6), 1414.
- Yin, G., Li, M., Wang, J. G., Xu, J., & Li, W. (2015). Mechanical behavior and permeability evolution of gas infiltrated coals during protective layer mining. *International Journal of Rock Mechanics and Mining Sciences*, *80*, 292–301. <https://doi.org/10.1016/j.ijrmms.2015.08.022>.
- Zhang, J., Ai, C., Li, Y.-W., Che, M.-G., Gao, R., & Zeng, J. (2018a). Energy-based brittleness index and acoustic emission characteristics of anisotropic coal under triaxial stress condition. *Rock Mechanics and Rock Engineering*, *51*(11), 3343–3360. <https://doi.org/10.1007/s00603-018-1535-9>.
- Zhang, Z., Wang, E., Li, N., Li, X., Wang, X., & Li, Z. (2018b). Damage evolution analysis of coal samples under cyclic loading based on single-link cluster method. *Journal of Applied Geophysics*, *152*, 56–64. <https://doi.org/10.1016/j.jappge.2018.03.014>.
- Zhang, H., Yin, X., Liang, N., Yu, H., Li, S., Wang, Y., et al. (2006). Acoustic emission experiments of rock failure under load simulating the hypocenter condition. *Pure and Applied Geophysics*, *163*(11), 2389–2406. <https://doi.org/10.1007/s00024-006-0129-8>.
- Zhang, C., & Zhang, L. (2018). Permeability characteristics of broken coal and rock under cyclic loading and unloading. *Natural Resources Research*. <https://doi.org/10.1007/s11053-018-9436-x>.
- Zhang, C., Zhang, L., Zhao, Y., & Wang, W. (2018c). Experimental study of stress-permeability behavior of single per-

- sistent fractured coal samples in the fractured zone. *Journal of Geophysics and Engineering*, 15(5), 2159–2170. <https://doi.org/10.1088/1742-2140/aac12e>.
- Zhang, Y., & Zou, Q. (2018). A prediction model for the slot depth of high pressure water jet. *Results in Physics*, 11, 1105–1109. <https://doi.org/10.1016/j.rinp.2018.11.020>.
- Zou, J., Chen, W., Yang, D., Yu, H., & Yuan, J. (2016). The impact of effective stress and gas slippage on coal permeability under cyclic loading. *Journal of Natural Gas Science and Engineering*, 31, 236–248. <https://doi.org/10.1016/j.jngse.2016.02.037>.
- Zou, Q., & Lin, B. (2018). Fluid–solid coupling characteristics of gas-bearing coal subjected to hydraulic slotting: An experimental investigation. *Energy & Fuels*, 32(2), 1047–1060. <https://doi.org/10.1021/acs.energyfuels.7b02358>.
- Zou, Q., Lin, B., Zheng, C., Hao, Z., Zhai, C., Liu, T., et al. (2015). Novel integrated techniques of drilling–slotting–separation–sealing for enhanced coal bed methane recovery in underground coal mines. *Journal of Natural Gas Science and Engineering*, 26, 960–973. <https://doi.org/10.1016/j.jngse.2015.07.033>.